Journal of Photochemistry and Photobiology A: Chemistry 209 (2010) 193–202

Contents lists available at ScienceDirect

Journal of Photochemistry and Photobiology A: Chemistry

journal homepage: www.elsevier.com/locate/jphotochem

Photolysis of methyl-parathion thin films: Products, kinetics and quantum yields under different atmospheric conditions

Michal Segal-Rosenheimer*, Yael Dubowski

Faculty of Civil and Environmental Engineering, Technion – Israel Institute of Technology, Technion City, Haifa 32000, Israel

ARTICLE INFO

Article history:
Received 12 August 2009
Received in revised form
12 November 2009
Accepted 21 November 2009
Available online 26 November 2009

Keywords:
Methyl-parathion
Photolysis
Quantum yields
Thin films
Atmospheric conditions

ABSTRACT

The present study focuses on the photodegradation of methyl-parathion thin films, an organophosphate insecticide, under different atmospheric conditions. The latter include nitrogenated, oxygenated and ozonated atmospheres, under low and high relative humidity conditions. Addition of oxygen to the atmospheric mixture did not seem to affect the reaction rates and quantum yields. Relative humidity affect was minor, with a small enhancement in reaction rate under 254 nm radiation. The addition of ozone (to either dry or humid atmosphere), at all concentrations tested, largely enhanced degradation rates. In the absence of ozone, the obtained quantum yields for photolysis of methyl-parathion thin films under 254 and 313 nm were 0.024 ± 0.007 and 0.012 ± 0.005, respectively. These values are higher than the values previously reported for solutions of methanol and water. Although the presence of molecular oxygen and water vapors did not seem to affect much the reaction rates, it did have a certain effect on the resulted products. More polar products were obtained under oxygenated and ozonated atmospheres, as well as dimers under ozone conditions. The reaction on thin films has yielded more toxic products than usually found in solutions, adding alkylphosphate esters in addition to the oxons formed normally.

1. Introduction

For the last couple of decades organophosphate pesticides (OPs) have been used abundantly on a vast range of insecticidal applications, from household and garden usage to commercial agricultural applications mainly on orchards and cotton grows [1,2]. Although their use has been decreased over the years, due to their high toxicity to mammals [3], OPs are still being used in large quantities. In Israel, for example, a recently published pesticides survey [4] has shown that OP usage has actually increased in 2006 in comparison to 2003.

The atmosphere is considered an important transportation medium for pesticides although most, including OPs, are semi-volatile compounds in nature [5–7]. Their introduction to the atmosphere is via drift during application, post-application volatilization and dust erosion. The amount volatilized from agricultural fields typically range between 20 and 50%, and sometime can even reach 90% for soil fumigants [8]. In addition to its importance with regard to pesticide transport, the atmosphere is also an important media for transformations of OPs [9–12]. As most OPs have low vapor pressure (e.g., 1.7×10^{-5} mmHg for methyl-parathion at 25 °C), they are susceptible to reside on airborne particles or deposited upon ambient surfaces [13]. Nevertheless, photochemical degradation of OPs has been studied mainly in aqueous solutions (e.g., [14–17], and references therein). Fewer studies were done involving OPs adsorbed onto soils [18–21], simulating soil under atmospheric conditions [18] or using theoretical simulations of atmospheric conditions [22]. Field observations [7,11] indicate that upon exposure to solar radiation and atmospheric oxidants organophosphates quickly degrade (within a matter of hours up to few days) from thion (P=S) to the oxon (P=O) active compounds, which are usually more toxic and soluble [23]. Woodrow et al. [24] exhibited a rapid conversion (within 2 min) of parathion to paraoxon at midday when released in the field. However, on testing parathion photochemical reaction in the gas-phase under controlled conditions they have observed conversion only after 40 min, and with the addition of ozone this time was shorten to half [25]. However, Winer and Atkinson [26] have shown that OPs gas-phase reaction with ozone was negligible. Apparent from the above, the radiation flux and the specific environmental conditions can significantly affect lifetime of the investigated pesticides. Moreover, the above investigations were conducted in the gas-phase. Hence, applying their findings to oxidation of sorbed semi-volatile pesticides is very limited as the kinetics of gas-phase and analog heterogeneous reactions can significantly differ [27,28]. The few previous studies regarding heterogeneous photoxidation of OPs indeed provided important information of relative reaction rates

* Corresponding author. Tel.: +972 4 8292808; fax: +972 4 8228898.
E-mail addresses: segalm@tx.technion.ac.il (M. Segal-Rosenheimer), yaeld@tx.technion.ac.il (Y. Dubowski).

1010-6030/$ – see front matter © 2009 Elsevier B.V. All rights reserved.
doi:10.1016/j.jphotochem.2009.11.014

Table 1
Summary of the different experimental set-ups.

Treatment	Radiation (254/313 nm)	N_2	O_2	RH[a]	O_3
a	+	+	–	–	–
b	+	+	+	–	–
c	+	+	–	+	–
d	+	+	+	+	–
e	+	+	+	–	+
f	+	+	+	+	+
a[b]	–	+	–	–	–
C[b]	–	+	–	+	–
e[b]	–	+	+	–	+
f[b]	–	+	+	+	+

[a] RH represents the conditions of high relative humidity during the experiment (values between 70 and 80% RH).
[b] Represents blank set-up, according to similar set-up with radiation.

[18] and possible surface products [29,30]. A new study regarding the photodegradation of methyl-parathion in ice has shown higher quantum yields compared to solutions [31]. Nevertheless, there is still a need for a more comprehensive studies on photolysis and quantum yields of surface bonded OPs, and of formation rates of their degradation products left on the surface and released to the air. Quantification of the photochemical processes under various atmospheric conditions, and the knowledge of their degradation products and formation rates will allow a better assessment of their atmospheric fate, and the possible impact on air quality and human health aspects.

Methyl-parathion (o,o-dimethyl o-p-nitrophenyl phosphorothioate) is an important member of the OP group, and was chosen as a model compound for the present study. The fact that its condensed photochemical degradation products are known, and that several investigations were made on it (mostly in aqueous phase) [16,18,32–39], make it an ideal compound for investigation and comparison.

The present work focuses on the investigation of photolysis of thin films of methyl-parathion under different atmospheric conditions (e.g., humidity, oxygen level, and presence of ozone), including reaction rates, quantum yields, and the formation rates of its degradation products.

2. Experimental

2.1. Experimental set-up and procedures

Detailed description of the experimental system is given elsewhere [40]. In brief, the system consists of a 45° Horizontal ZnSe ATR crystal (HARTPlus, Pike Technologies Inc.) placed in a flow-through homemade Stainless steal chamber with a quartz window at its top. A mercury lamp (model 3UV lamp-38, 8 W UVP, Ltd.) was placed on top the quartz window. Illumination central wavelengths were at 254 or 313 nm.

Photodegradation of methyl-parathion thin films was tested under various conditions as summarized in Table 1. Settings 'a–f' has been conducted both under 254 and 313 nm radiations. A set of blank experiments with no radiation was conducted under all selected gas mixtures as detailed in Table 1 (i.e., settings a[b], c[b], e[b], and f[b]). In the table, RH refers to high relative humidity atmosphere (i.e., 70–80% for high RH and below 5% otherwise). Humidification was obtained by bubbling dry nitrogen gas through DI water (18.2 MΩ water, Millipore). Relative humidity and temperature of the gas flow were monitored in a mixing cell located just before the reactor's inlet, using AHLBORN Alemo® 2390-3 instrument. Temperature ranged between 22.2 and 25.3 °C. N_2 and O_2 (both, >99.999% Maxima) mixture at a ratio of 4:1, was used as a synthetic atmosphere. Ozone was generated by irradiating a dry flow of O_2 and He (both >99.999%, Maxima) with a low-pressure mercury lamp emitting at 185 and 254 nm (Jelight Inc., double bore 78-2046) and then was measured with an ozone monitor (InDevk, 2B Technologies). Working concentrations were between 7×10^{12} and 2×10^{14} molecules/cm^3, which corresponds to 300 ppb to 10 ppm. High concentrations were used in some of the 254 nm experiments for a better detection and identification of products, where lower concentrations (~300 ppb) were used under the 313 nm experiments to resemble more closely atmospheric scenarios such as heavily polluted atmosphere. Methyl-parathion film was deposited directly on the ATR crystal by applying 100 μl of 3 mM solution of the pure compound (Supelco, Neat grade) in ethanol (BioLab, analytical reagent) and allowing the solvent to evaporate (complete removal of the solvent was confirmed by ATR spectra). The ATR flow-through chamber was then sealed to ambient atmosphere. Spectral measurements started simultaneously with the mounting of the UV lamp on top of the chamber's quartz window, while the proper gas mixtures were flowing continuously through it. Total flow was kept constant under all experimental conditions. Radiometric readings were taken using 254 and 313 nm calibrated sensors (UVX Radiometers by UVP), that were mounted (in separate experiments) at the same location, distance and configuration as the ATR crystal in the experimental system. Irradiance measurements gave 542 and 391 μW/cm^2, for the 254 and 313 nm lamps, respectively.

Infrared absorbance spectra averaged 32 scans per spectrum at 2 cm^{-1} resolution over a spectral detection range of 4000–650 cm^{-1}. Background was taken on a clean ATR crystal under the corresponding experimental conditions.

Absorption cross-section of the methyl-parathion film was determined by measuring its absorbance at varying surface concentrations. Films were deposited in a defined slot on a quartz slide, and their absorbance was measured between 200 and 600 nm (resolution of 2 nm) using UV–vis spectrophotometer (Genesis 10 UV, Thermo®).

2.2. GC–MS analysis

Residue of the reacted methyl-parathion film was extracted at the end of the experiments with 3 ml of ethanol (BioLab, analytical reagent) and analyzed by gas chromatography–mass spectroscopy (GC–MS) for the verification and identification of surface photoproducts. For identification, 5 μl samples were injected into the GC–MS (Varian CP-3800 GC with MS trap detector Varian Saturn 2000, run in EI mode). Injector temperature was 240 °C and analysis was done using a capillary column (Varian DB-5 column; 30 m; 250 μm I.D.; film thickness 0.25 μm). The method started at 50 °C, which was held for 2 min, then ramped to 100 °C at a rate of 20 °C/min, followed by an increase to 150 °C at 5 °C/min, and then to 250 °C at 10 °C/min. The method used an initial splitless mode and a split ratio of 1:10 after 1 min. Ions were collected in the range of 40–300 *m*/*z*.

3. Results and discussion

3.1. Methyl-parathion photolysis rates under various atmospheric conditions

Fig. 1 shows the spectral changes observed during photolysis of methyl-parathion film under 254 nm irradiation and dry oxygenated atmosphere.

3.1.1. Spectra interpretation

Representative bands of the parent molecule are shown in Fig. 1. The vibrational frequency of the P=S band is usually about 675 cm^{-1}. However, the symmetrical stretching frequency of the PO_3 group is known to interact mechanically with this

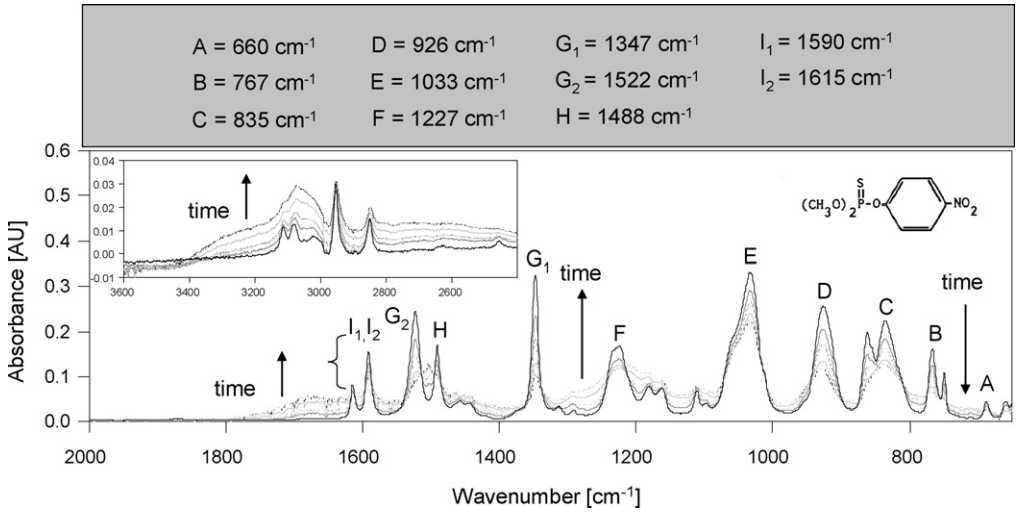

Fig. 1. Temporal changes of methyl-parathion film during photolysis under 254 nm in dry oxygenated atmosphere. Insert shows increase with time of the 2400–3600 cm^{-1} region. Methyl-parathion (solid black line) representative bands are shown in panel above. A detailed assignment for the functional groups is given in text.

band and obscure its specific location [41]. Following this, bands A (660 cm^{-1}), B (767 cm^{-1}), and C (835 cm^{-1}) were assigned, respectively, to the P=S stretch, PO_3 symmetric stretch, and PO_3 asymmetric stretch vibrations within the conjugated bond of O_3P=S. Bands D (926 cm^{-1}) and E (1033 cm^{-1}) were assigned to the P–O stretch vibration of the P–O–Ar (Ar = aromatic ring) group, and to the O–C stretch of the P–O–CH_3 group, respectively. B and F (1227 cm^{-1}) were assigned to the O–Ar stretch whereas bands G_1 and G_2 were assigned to the symmetric and asymmetric stretching of the NO_2 group [42]. H band at 1488 cm^{-1} represents the *para* substituted benzene ring, and finally, the I_1 and I_2 bands were assigned to the stretch vibrations of the di-substituted benzene [41].

3.1.2. Kinetics

As exposure time increases, the absorbance at the bands assigned to the parent molecule, as detailed above was decreasing. It can be noticed that many of the original bands exist also in the product molecules. Hence, methyl-parathion loss rate can be extracted only from its unique bands at 767 and 660 cm^{-1} (B and A in Fig. 1). The latter, however, was not used as a proxy for the reaction rate measurement due to its low intensity, and its higher susceptibility to measurement noise (detection threshold of our IR detector was at 650 cm^{-1}).

Photolysis rate constants were extracted from the fit of temporal changes in absorbance peak area at the 767 cm^{-1} band. All the analyzed data fit an exponential decay model (p-value < 0.001), indicating first order kinetics. Blank experiments (noted as a–f^b in Table 1) revealed a certain amount of methyl-parathion volatilization under the different experimental settings and although methyl-parathion has a relatively low vapor pressure, other investigations [18] also showed differing amounts of volatilization under different conditions. In the present case, however, volatilization rates were similar under the different settings (0.0019 ± 0.0002 min^{-1}) and their averaged value was subtracted from the observed decomposition rate constant to yield the net photolysis rate constant k_p for each setting. Temperature variation during experiments was negligible (1 and 0.3 °C over 4 h of irradiation for 254 nm, and 313 nm light, respectively), and hence, was not considered to affect evaporation rate. Photolysis rates and half-lives for all tested conditions are summarized in Table 2. Half-lives were calculated based on the first order photolysis rate constants ($t_{1/2} = \ln 2/k_p$). Photolysis rates under the 254 nm irradiation were higher by a factor of two to three when compared to the rates under 313 nm light, at the same experimental conditions. Photolysis rates under dry nitrogenated or oxygenated atmospheres did not show significant difference. Previous investigations regarding parathion photolysis [13] indicated that the presence of water can contribute to the thion to oxon conversion via interaction of water molecules with the synthesized parent molecule or with reactive intermediates. Comparison between the photolysis rates observed in the present study under humid and dry conditions showed indeed a small enhancement under humid nitrogenated atmosphere and 254 nm light. Under all other conditions the differences were within experimental error.

Although MPT is not very reactive towards ozone [26], the presence of ozone did seem to significantly enhance the photolysis rates of methyl-parathion. In comparison to our blank experiments with ozone (e^b and f^b in Table 1), direct reaction of MPT with ozone could not explain the relatively high photolysis rates, both under 254 and 313 nm radiations (i.e., $k[e^b] + k[b] \ll k[e]$), indicating a synergistic effect between UV and O_3, as also observed by Kromer et al. [18]. The enhanced rate can be a result of an indirect photolysis pass involving the photochemical decomposition of ozone under UV radiation (where wavelengths up to 313 nm are effective) to molecular oxygen in its singlet state $O_2(^1\Delta_g)$, and to electronically excited oxygen $O(^1D)$ [27]. Both species are reactive and can induce the formation of carboxylic moieties and ketones from aromatic alcohols. This assumption is supported later on by our spectral and chromatographic product analysis. As no significant difference was observed between dry and humid conditions in the presence of

Table 2
Methyl-parathion films photolysis rates (min^{-1}) under the different experimental set-ups (half-lives in minutes are shown in parenthesis).

	a	b	c	d	e	f
254 nm[a]	0.0027 ± 0.0007 (261)	0.0025 ± 0.0004 (278)	0.0032 ± 0.0009 (215)	0.0021 ± 0.0008 (324)	0.0038 ± 0.0003 (183)	0.0038 ± 0.0003 (183)
313 nm[a]	0.0010 ± 0.0006 (702)	0.0011 ± 0.0006 (630)	0.0011 ± 0.0002 (630)	0.0008 ± 0.0002 (880)	0.0016 ± 0.0002 (437)	0.0019 ± 0.0004 (358)

[a] Radiation experiments under 254 nm were done in triplicates ($n = 3$), and under 313 in duplicates ($n = 2$) for each setting. Error values correspond to deviation between replicates.

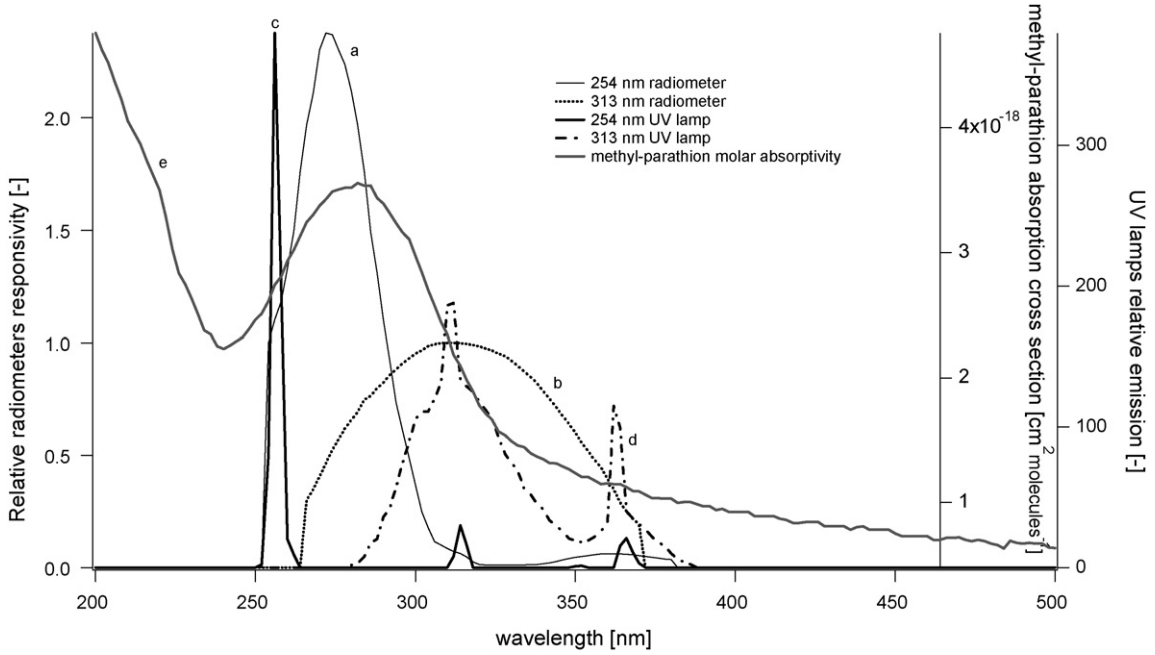

Fig. 2. Relative spectral responsivity curves of (a) 254 nm radiometer, (b) 313 nm radiometer, and the spectral illumination curves of (c) 254 UV lamp, (d) 313 UV lamp used in the laboratory experiments, and (e) absorption cross-section curve of methyl-parathion thin film. UV lamps and radiometer responsivity curves are given in relative units.

ozone at 254 nm radiation, the existence of hydroxyl radicals was considered to be of a minor effect.

The obtained photolysis rates and half-lives are difficult to compare with other studies due to the large difference in reaction conditions and set-ups. Hence, quantum yields were calculated for the different experimental set-ups and were used for comparison.

3.2. Methyl-parathion quantum yields under various atmospheric conditions

Quantum yields were calculated by using the following equation:

$$\Phi = \frac{dC/dt}{I_{abs}} \tag{1}$$

where dC/dt is the observed initial photodegradation rate (the extracted k_p), and I_{abs} is the light flux absorbed by the methyl-parathion film. I_{abs} is a function of both the incident light flux (I_0) and the average absorption cross-section coefficient $\langle \varepsilon \rangle$ (cm^2/molecule). I_0 was calculated from the light flux measured using the specific radiometers for each lamp and a correction factor compensating for the differences between spectral illumination curves of the UV lamps and the spectral responsivity curves of the corresponding radiometers (see detailed explanation in Segal-Rosenheimer and Dubowski [40]). $\langle \varepsilon \rangle$ was calculated over the spectral range of the radiometers (λ_1–λ_2 were in the ranges of 254–370 and 266–370 nm, for the 254 and 313 nm UV lamps, respectively) according to:

$$\langle \varepsilon \rangle = \frac{\int_{\lambda_1}^{\lambda_2} I(\lambda) \times \varepsilon(\lambda) d\lambda}{\int_{\lambda_1}^{\lambda_2} I(\lambda) d\lambda} \tag{2}$$

where $I(\lambda)$ represents the lamp spectral output function (see Fig. 2) and $\varepsilon(\lambda)$ is the measured absorption cross-section of methyl-parathion film at wavelength λ, as shown in Fig. 2. Following the above, the actual light flux initially absorbed by the methyl-parathion film (I_{abs}) is given by:

$$I_{abs} = I_0 \times \langle \varepsilon \rangle \times [C]_0 \tag{3}$$

where $[C]_0$ is the initial methyl-parathion thin film surface concentration in molecules/cm^2. Similar film thickness was assumed on both ATR experiments and on absorption cross-section measurements.

Since photodegradation rates of methyl-parathion was relatively similar under the different atmospheric conditions (except under ozonated atmosphere), the obtained quantum yields are given as an averaged value (with their standard deviation) for each radiation wavelength. Values obtained following the above calculations yielded quantum yields of 0.024 ± 0.007 and 0.012 ± 0.005 for 254 and 313 nm radiations, respectively. These values are an order of magnitude higher than the values published by Wan et al. [17] for methyl-parathion in methanol (data available only for 254 nm radiation), and are 50 times higher than the corresponding values of methyl-parathion quantum yields in water (both for 254 and 313 nm radiations). Nevertheless, the relative ratio between the 254 and 313 nm quantum yields in the present study (~2) corresponds well with the ratio published by Wan et al. for aqueous solution [17]. Recent values published by Weber et al. [31] has shown that quantum yields in ice were at least 6 times higher than the values obtained by Wan et al. in aqueous solutions [17], with no apparent difference between aerated and degassed conditions. Their values were obtained at the low temperatures of −20 °C, in comparison to the present study, which was held under ambient temperatures (~25 °C).

According to the quantum yield obtained under 313 nm light, the outdoor half-life of methyl-parathion films can be evaluated. It appears that the flux of solar radiation greatly affect this environmental parameter, which range between 80 min, at a solar zenith angle (SZA) of 10° (corresponding to midsummer at our location, 32°N,) to 30 h (1.3 days) for SZA of 86°. Such half-lives and wide fluctuations were observed previously in many outdoor and laboratory investigations regarding the photolysis of OPs and are detailed in a review paper by Floesser-Mueller and Schwack [13]. The fact

that observed degradation rates could vary between hours to days and even weeks, further emphasize the importance of obtaining quantum yields rather than half-lives. The large variability in the basic radiation conditions (throughout the day), accompanied by different environments (different humidity, ozone levels, different surfaces, etc.) can indeed cause large differences in final half-lives obtained in the field. Chukwudebe et al. [29] have found that 70% of methyl-parathion thin films were degraded under solar radiation after 14 h. However, they did not supply any information regarding the time of year or of the total radiation flux to allow proper comparison with our current results. In comparison to a former investigation done by our group on the photolysis of cypermethrin [40] (an insecticide of the pyrethroid family), it was shown that under SZA of 10° the half-life of this compound will be around 19 h. Although quantum yields for methyl-parathion were found to be lower than for cypermethrin, its absorption spectrum has higher overlap with solar spectrum, grading it as a more sensitive compound to photolysis in comparison to cypemethrin.

3.3. Photoproducts

3.3.1. Products identification by GC–MS

Many investigations have shown that the formed degradation products of organophosphates, especially of parathion ([13] and references therein) were not affected by the UV radiation wavelengths used (254 or 313 or 365 nm). Indeed, our results support this observation as same products were identified on both radiations used in the present study.

Two surface products, methyl paraoxon (MPO) and o,o,s trimethyl-thiophosphate (OTT) were identified by our GC–MS analysis under all experimental conditions, with lower OTT to MPO ratio when O_3 was also present (i.e., settings e and f). MPO is a well documented photoproduct of methyl-parathion (e.g., [13,16] and references therein), while OTT is the methyl analog of one of the well known photoproducts of ethyl-parathion [13], o,o,s triethyl-thiophosphate, and was also detected as a main photoproduct of methyl-parathion thin films under sunlight and UV radiation [29]. In addition to these two surface products other products were found under specific conditions (see also Scheme 2). Methanecarbothiolic acid (MCA) was detected under all conditions, except for dry nitrogen (setting a). Additional polar products were observed under humid and oxygenated conditions, including: the aliphatic acid 2-propionic acid, 2 methyl (AA), propanoic acid (PA), and alcohols (2-propyl 1-pentanol, 2PP). Diethyl-phthalate (DiePH) and dimethyl phthalate (DimPH) were detected after irradiation under dry oxygen and dry ozone, respectively. Furthermore, p-(2,2,4-trimethyl-4-chromaryl) phenol (TCP) was detected only in the presence of O_3 (i.e., settings e and f).

It is worth noting that our GC analysis is likely to underestimate the formation of carboxylic acids and aldehydes since no derivatization was used.

3.3.2. Spectral product identification and reaction trends

Spectral analysis of the temporal changes during reaction revealed some additional insights regarding products formation, and supported some of our GC–MS analysis results. Fig. 3 shows the spectral changes occurred during photolysis under the oxygenated conditions (settings b and d–f, the other conditions are not shown for clarity). Fig. 3A focuses on the spectral region between 650 and 1900 cm^{-1}, and Fig. 3B focuses on the region of 2800–3800 cm^{-1}. Upon exposure to UV light, under all tested gas mixtures, increased absorbance was observed in the following bands (Fig. 3A lower part): 791 cm^{-1}, between 800 and 880 cm^{-1}, 1200 cm^{-1} (broad increase including 1187, 1263, and 1294 cm^{-1} bands), 1488, 1524 cm^{-1}, and the bands between 1640 and 1780 cm^{-1}. The latter are especially enhanced under ozonated

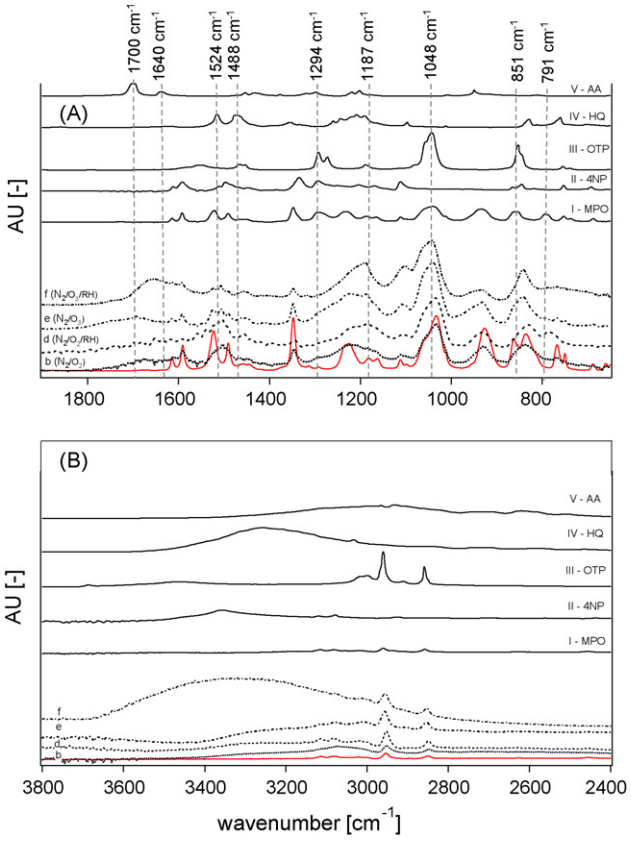

Fig. 3. Spectra of the photolysis reaction of methyl-parathion under various atmospheric settings (b–f, as detailed in Table 1) at the end of each experiment for the spectral ranges of (A) 650–1900 cm^{-1} and (B) 2800–3800 cm^{-1}. Initial spectrum of methyl-parathion is shown as red solid line at the bottom of each panel. Standard spectra (taken from NIST spectral library) of the photoproducts of methyl-parathion that were used for spectral analysis are shown in the upper part of each panel. Spectra were shifted for clarity.

conditions. This region represents carbonyl absorption bands associated with aldehydes, ketones and carboxylic acids, and hence increase more prominent under oxygenated conditions (ozone or oxygen, with higher intensity under ozonated conditions) in comparison to only nitrogen atmospheres (spectrum not shown). The PO_3 symmetric stretch of the $O_3P{=}O$ band (791 cm^{-1}), and the P=O band stretch (1294 cm^{-1}) can be associated to methyl paraoxon (MPO, spectrum I in upper panel in Fig. 3A), and the latter also to o,o,s trimethyl-thiophosphate (OTT). Since reference standard or library spectrum of OTT was not available, the spectrum of o,o,o trimethyl-phosphate (OTP) was selected to spectrally represent it (spectrum III in upper panel of Fig. 3A). Both compounds are almost similar, apart from the difference in their P–S (OTT) and P–O (OTP) bonds that have spectral contribution around 613–440 cm^{-1}, out of our measure spectral range [41]. The relatively broad band increase at the 800–880 cm^{-1} emerging together with the decrease of the representative bands of the parent molecule can explain the increase of both MPO and OTT. Although OTP was not detected in our GC analysis, it is also known as one of the possible photoproducts of methyl-parathion [29]. The 1297, 1640, and the 1700 cm^{-1} bands in the photolyzed MPT film can be associated to the aliphatic acid detected (AA) (spectrum V). Although not detected by our GC–MS analysis, the signature of hydroquinone (HQ, spectrum IV) can also be detected in the spectrum of photolyzed MPT film (Fig. 3A), both at the broad 1200 cm^{-1} band and at the 1488 cm^{-1} band, which represents *para* substituted benzene rings [41]. Also, its contribution can be seen at the 3000–3400 cm^{-1} OH band stretch (Fig. 3B). The fact that 4-nitrophenol (4NP, spectrum II) was not

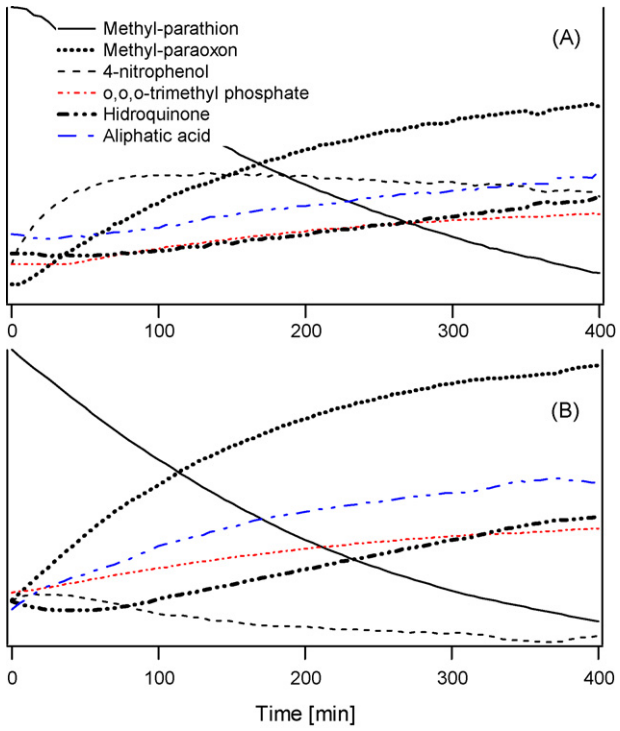

Fig. 4. Reaction progress plots of methyl-parathion and its products using the "inverse model" calculations, as detailed in the text (*y*-axis represents relative progress, and hence is unit less). Panel (A) represents reaction progress under dry oxygenated atmosphere and panel (B) is under dry ozonated atmosphere.

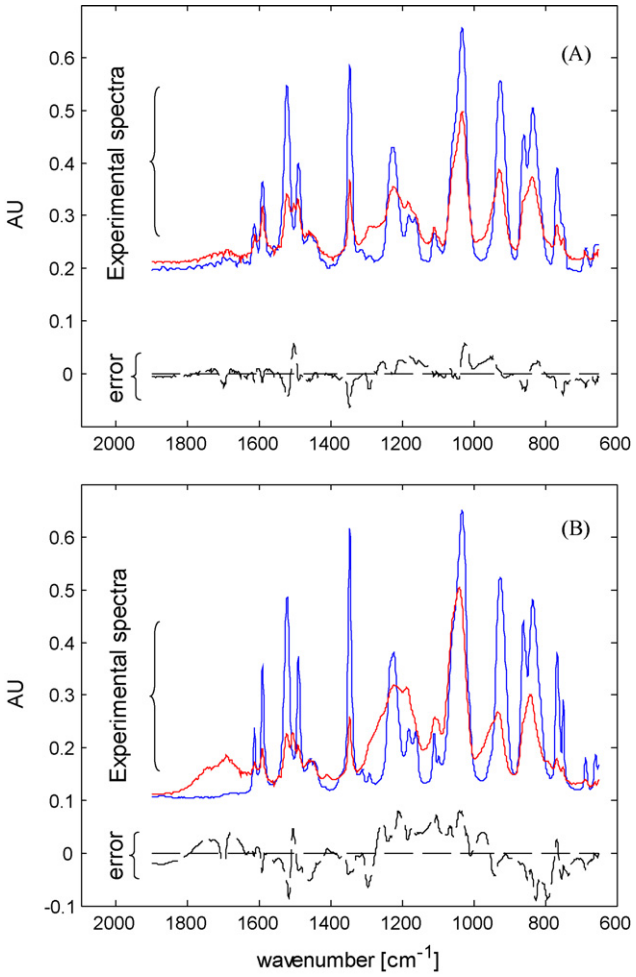

Fig. 5. Experimental spectra of the initial methyl-parathion film (solid blue line) and final residue after photolysis at 254 nm (dotted red line) at dry oxygenated atmosphere (A) and dry ozonated atmosphere (B). Black lines represent the reconstruction error as detailed in text. (For interpretation of the references to color in this figure legend, the reader is referred to the web version of the article.)

detected in the GC–MS and spectral analyses of the films' residue at the end of the experiments may in part be a result of its susceptibility to direct photolysis [13]. Indeed, as will be shown later (Fig. 4), the continuous FTIR analysis does show its build-up and loss during the reaction. The recent study by Weber et al. [31] also mentioned its relatively low formation yields and its susceptibility to photolysis, making it difficult to trace it at the end of reaction.

Upon photolysis an increase in the OH associated band (3000–3600 cm^{-1}) is observed as well as a smaller increase at the 2800–3200 cm^{-1} region. Comparing the different experiments, it seems that under dry oxygen conditions, the broadening occurs mainly in the 2800–3200 cm^{-1} range, while under humid conditions, the OH broadening is up to 3400 cm^{-1}. Similar behavior is seen upon irradiation in the presence of ozone, when dry atmosphere results in a broadening up to 3400 cm^{-1} and a humid atmosphere results in a very broad peak up to 3600 cm^{-1}. These trends probably represent both the formation of acid products (mainly under humid oxygenated atmosphere) and an increase in surface hygroscopicity following the formation of more polar photoproducts. In the presence of ozone, photo-oxidation results in even higher water uptake (under high RH experiment), which increases absorbance in the bulk water band of 3400 cm^{-1}.

The contribution of the OTT/OTP band at around 3000 cm^{-1} can be seen under all experimental settings. Also, HQ contribution seems to be more prominent under humid conditions. The spectral signature of 4NP, which acts more as an intermediate, cannot be seen clearly in the presented end-of-experiment spectra. The broadening of the absorption bands around 3200–3400 cm^{-1} under settings b, d and e could be explained quite well with the identified products. However, the large broadening under setting f (humid ozonated atmosphere) could not be attributed to the known spectral features of the detected and postulated products. As mentioned earlier, additional products were found to prevail under ozonated conditions (e.g., TCP), but their reference spectra were not available. Furthermore, enhanced water uptake by the oxidized film may also affect this spectral region.

The five products shown in Fig. 3 were used to reconstruct the temporal reaction spectra, using the "inverse method", as described in Segal-Rosenheimer and Dubowski [40]. In short, the obtained temporal spectra are assumed to be superposition of both the parent material (i.e., methyl-parathion), and its photodegradation products. A linear decomposition was obtained over the "fingerprint" spectral range of 650–1900 cm^{-1} using least square minimization to find the best fit of the spectral contribution of parent material and its products at each time point. This analysis gave an insight on the changes of the parent material and its products with time, as shown in Fig. 4. The amount of each component is described as the ratio relative to its reference spectral signature, and the trend in time can be quantified to give the formation or loss rates. Decrease rates of methyl-parathion calculated this way correlated quite well with its decomposition rates calculated based on the 767 cm^{-1} band. The general trends of the reaction progress under all conditions were very similar. The loss rates of MPT were similar to obtained formation rates for OTT but slower than the calculated formation rates of MPO. This is not too surprising considering that the latter was estimated based on the absorbance band associated with the O=(P–O_3)–Ar, and it is likely that additional unaccounted products with similar functional group (and spectral signatures) are present and resulted in overestimation of MPO

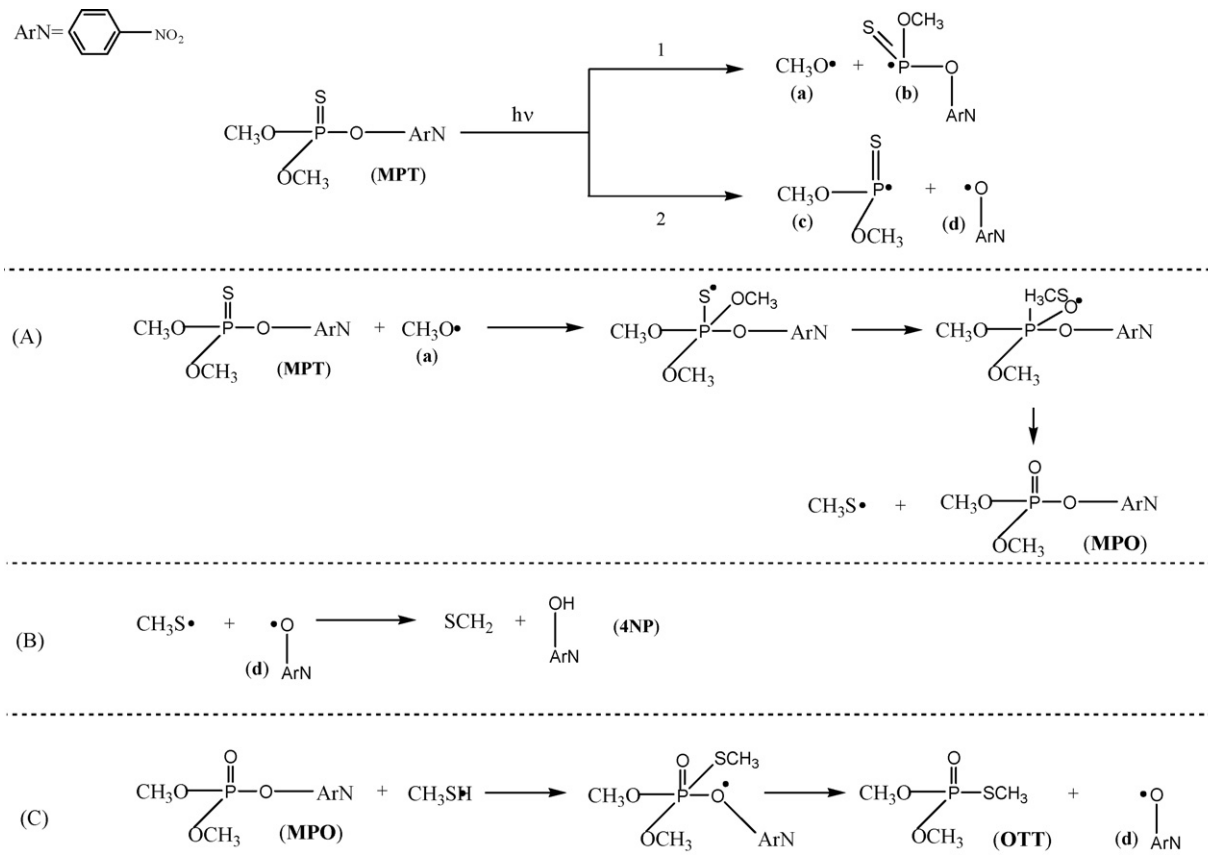

Scheme 1. Pathways of the main three photoproducts for methyl-parathion photolysis on thin films.

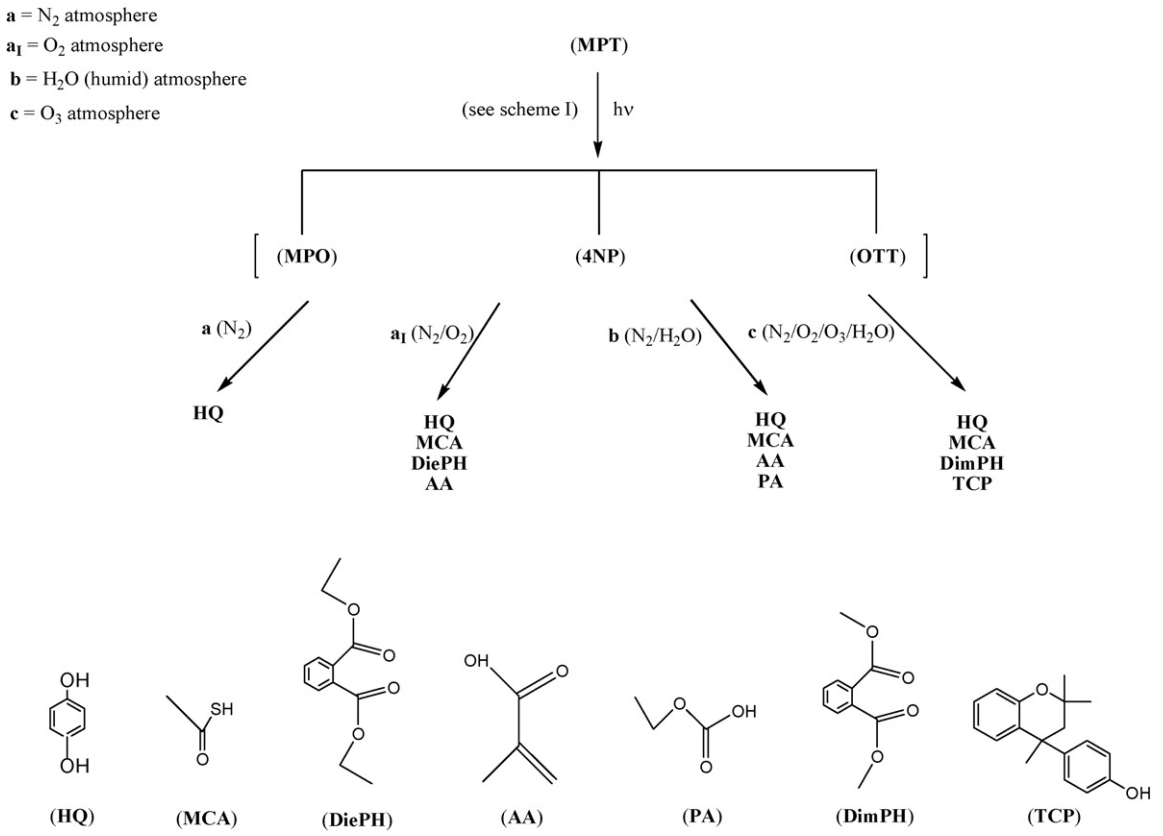

Scheme 2. Secondary photoproducts formation under the different experimental atmospheric settings.

formation rate. Degradation products with such functional group (although not identified in the present study) can be attributed to denitroparaoxon, and o-methyl, o,o-bis(4-nitrophenyl) phosphate, as were suggested in the past [13,30,43]. 4NP seems to be formed and degrade during reaction, which can explain its absence at the end of reaction from the IR spectrum and from the GC chromatogram. Also, it can be noticed that like for MPT, the degradation of 4NP under radiation and ozone (Fig. 4B) occurs faster than in the absence of ozone (Fig. 4A). Initial formation rate of 4NP was slower than the decrease rate of methyl-parathion (MPT), which supports its formation as a secondary product. Formation rate of HQ was also slower than MPT degradation rate and supports its formation as a secondary product, most probably of 4NP photolysis [16]. HQ build-up was noted to increase faster when ozone was present.

Spectral reconstruction was obtained to test the accuracy of the "inverse model" solutions. The reconstructed spectrum was based on the coefficients extracted via the least square fit to yield a calculated spectrum. Then, at each time point, the calculated spectrum was subtracted from the measured spectrum. Fig. 5A and B presents the results of this procedure for the same experiments shown in Fig. 4 (oxygenated and ozonated, respectively). The main deviations can be observed around the 800, 1290, 1000–1200, and 1650–1750 cm^{-1} absorption bands, where the negative error in the first two indicate an overestimation of the products absorbing at this location (i.e., methyl paraoxon). In general, Fig. 5A, which represents the reconstruction error under oxygenated conditions, shows smaller deviations when compared to Fig. 5B (ozonated atmosphere). A larger positive reconstruction error is shown under ozone atmosphere, especially at the 1650–1750 cm^{-1}, and the 1000–1200 cm^{-1} band regions. The above regions are associated with carbonyl functional groups, and ether–ester moieties, respectively. Their positive deviation implies that there are still additional compounds which were not accounted for in the reconstruction procedure and enhances our assumption that our GC analysis did not result in the full assembly of photoproducts. Also, as postulated previously [44], the increased absorbance between 1100 and 1200 cm^{-1} can represent dimmer formation due to surface radical reactions.

IR analysis of the gas downstream the reaction cell indicated the presence of carbon dioxide, carbon monoxide (CO), and unidentified gas products containing carbonyl groups.

3.4. Suggested reaction pathways

Photolysis mechanisms of OPs, especially of aromatic thiophosphates, were investigated (to the best of our knowledge) only in solutions [13]. The two known mechanisms are related to different types of solvents; polar and non-polar; the former involves ionic interactions, while the latter involves radical reactions. In our case, as thin films are involved, the basic mechanism is postulated to be controlled by radical reactions. The alkoxy radicals formed upon the breakage of the exited MPT molecule may react (see Scheme 1) with the parent molecule or its fragments and lead to the formation of MPO, 4NP, and OTT (see the three paths in Scheme 1). The production of OTT is postulated to result from the interaction of the initial photolysis fragments of MPT and MPO [13], as shown in Scheme 1.

Under various atmospheres different products emerge (Scheme 2) due to secondary reactions involving MPO, 4NP and OTT. The three suggested pathways support the formation of the three main photoproducts under all atmospheric conditions, as indeed was shown in our analysis.

HQ is postulated to be formed either by the photolysis of 4NP leading to unimolecular cleavage of the C–N aromatic bond, followed by reaction with H_2O or with OH radicals [13,45]. The latter can be generated here via secondary radical reactions, or in some cases by the direct decomposition of aromatic-nitro groups [31], which are present here. Under non-humid conditions (N_2 and N_2/O_2 atmospheres), the reaction progresses via a pathway a in Scheme 2, similar to the description of the pathway under degassed non-protic media [13], involving the initially produced alkoxy radicals (a and d in Scheme 1). Under oxygenated atmosphere the additional formation of peroxy radicals may occur, which then yield additional polar degradation products (pathway a_1 in Scheme 2). In our observations, oxygenated atmosphere did not affect the reaction rate, but have added the additional oxygenated products. Addition of water vapor seemed to result in the production of carboxylic acid moieties. Also, under oxygenated and ozonated conditions, the formation of larger molecules, such as DiePH, DimPH, and TCP can be the result of the combination of two monomers on the surface. In the case of ozonated atmosphere (pathway c in Scheme 2), the initial excitation step is postulated to yield the alkoxy radicals (a and d in Scheme 1). However, as ozone undergoes photolysis to produce singlet oxygen and excited oxygen atom [27], it may accelerate reactions following the first excitation step due to additional production of peroxy and secondary hydroxyl radicals (formed mainly via secondary reactions). It is interesting to note that increasing ozone levels did not affect significantly the overall reaction rate, strengthening the conclusion that ozone does not react directly with the MPT molecule, but only via its role in the formation of secondary radicals. Surface ozone coverage was probably at saturation under all ozone concentrations used in the present study ($\geq$300 ppb). The observed lack of dependency of degradation kinetic on gaseous ozone level also suggests that photolysis of gaseous ozone followed by atomic oxygen chemistry was of less importance than the photolysis of adsorbed ozone, at the limit of saturated surface coverage. Indeed, Kromer et al. [18], who worked with lower ozone levels (85–200 ppb), did report an increase in reactivity towards higher levels of ozone. The high formation of radicals (under relatively high ozone levels) can also result in an increasing rate of terminating reactions.

4. Conclusions

Although post-application photolysis of MPT is expected to occur mainly when it is adsorbed at the solid–air interface, quantitative information on this heterogeneous process is scarce. The present study investigates the photolysis of methyl-parathion thin films under various atmospheric conditions. The chemical changes in the film upon irradiation were monitored in real-time using ATR-FTIR spectroscopy, providing information on the kinetics and surface product formation. To the best of our knowledge, this is the first time quantum yield values are reported for photolysis of MPT sorbed on inert surfaces. The obtained quantum yields were almost insensitive to the different atmospheric conditions tested (nitrogen or oxygenated, under dry or humid conditions), suggesting that the same value can be used for estimating the photodegradation of sorbed MPT over a relatively wide range of ambient atmospheric conditions. Although the obtained quantum yields of MPT films were higher than previously reported in solutions, the ratio between 254 and 313 nm quantum yields were shown to be similar.

It was also shown that ozone significantly affects the overall photolysis pathway. As the direct reaction of ozone with parent material is slow, the observed synergistic effect of ozone and UV is attributed to enhanced secondary reactions due to the formation of peroxy radicals. The presence of ozone also contributes to the formation of polar products (ketones, aldehydes, and carboxylic acids), which in turn results in higher water uptake of the film, as suggested by the enhanced absorbance in the broad OH bands around 3400–3600 cm^{-1} following photo-oxidation under humid

conditions. Under dry conditions, the bounded OH region was concentrated mainly at the region up to 3200 cm^{-1}, and was attributed to the formation of carboxylic acids.

Using a linear combination of the IR spectra of the parent compound and of the identified products, the observed temporal spectra were reconstructed. These reconstructed spectra allowed us to continuously follow the formation and loss rates of the parent compound and its photoproducts. The largest error in the reconstruction spectra was identified under ozone conditions supporting our assumption that our GC–MS analysis underestimated certain photo-oxidation products, such as carbonyls, esters, and possible surface dimmers (absorbing around 1100–1200 cm^{-1}). Nevertheless, under all other tested conditions, reconstruction error was relatively small; up to 10% at all times, suggesting that the identified photoproducts (based on GC–MS and infrared spectral analysis) are the predominant species for the investigated reaction.

Relative humidity seemed to have a minor effect in the present investigation. Although it did seem to slightly enhance reaction rates under nitrogenated atmosphere, as was reported previously [13], the mutual effect of both oxygen and high relative humidity did not seem to yield higher rates.

One of the major concerns regarding the environmental fate of OP pesticides is their toxicity and the toxicity of their degradation products. Most studies of photochemical degradation of methyl-parathion in aqueous solution indicated 4-nitrophenol and methyl paraoxon as the major photoproducts. The present work, like previous studies on photolysis of sorbed MPT (e.g., Sakellarides et al. and Chukwudebe et al. [21,29]) indicate significant formation of additional surface products; including trimethylphosphorothioate esters that are known to have delayed toxic effect.

Acknowledgments

This research was funded by Marie Currie International Reintegration grant, as part of the sixth framework programme of the European Commission, and the Israeli Ministry of science, through the Levi Eshkol fellowship.

References

[1] V. Feigenbrugel, A. Le Person, S. Le Calve, A. Mellouki, A. Munoz, K. Wirtz, Atmospheric fate of dichlorvos: photolysis and OH-initiated oxidation studies, Environmental Science & Technology 40 (2006) 850–857.
[2] E.D. Richter, P. Chuwers, Y. Levy, M. Gordon, F. Grauer, J. Marzouk, S. Levy, S. Barron, N. Gruener, Health effects from exposure to organophosphate pesticides in workers and residents in Israel, Israel Journal of Medical Sciences 28 (1992) 584–598.
[3] T.R Fukuto, Mechanism of action of organophosphorous and carbamate insecticides, Environmental Health Perspectives 87 (1990) 245–254.
[4] Y. Bar-Ilan, G. Malman, Usage Survey of Pesticides in the Lake Kinneret Basin—2006 Period, 2007, pp. 1–92.
[5] H. de-ruiter, H.J. Holterman, C. Kempenaar, H.J.L. Mol, J.J. de-Vlieger, J.C.V. de-Zande, Influence of Adjuvants and Formulations on the Emission of Pesticides to the Atmosphere, Plant Research International B.V., 2003.
[6] M. Harnly, R. McLaughlin, A. Bradman, M. Anderson, R. Gunier, Correlating agricultural use of organophosphates with outdoor air concentrations: a particular concern for children, Environmental Health Perspectives 113 (2005) 1184–1189.
[7] M.S. Majewski, M.M. McChesney, J.E. Woodrow, J.H. Prueger, J.N. Seiber, Aerodynamic measurements of methyl-bromide volatilization from tarped and nontarped fields, Journal of Environmental Quality 24 (1995) 742–752.
[8] F. Van den Berg, R. Kubiak, W.G. Benjey, M.S. Majewski, S.R. Yates, G.L. Reeves, J.H. Smelt, A.M.A. van der Linden, Emission of pesticides into the air, Water Air and Soil Pollution 115 (1999) 195–218.
[9] J. Seiber, S. Datta, J. Woodrow, Transport and fate of pesticides in fog in California's Central Valley, Abstracts of Papers of the American Chemical Society 215 (1998) U37–U137.
[10] J. Seiber, J. LeNoir, C. Wujcik, J. Woodrow, Atmospheric deposition or organic contaminants in the Sierra Nevada mountains and the Great Basin, Abstracts of Papers of the American Chemical Society 214 (1997) 82–90.
[11] J.N. Seiber, B.W. Wllson, M.M. McChesney, Air and fog deposition residues of four organophosphate insecticides used on dormant orchards in the San Joaquin Valley, California, Environmental Science & Technology 27 (1993) 2236–2243.
[12] P.S. Honaganahalli, J.N. Seiber, Measured and predicted airshed concentrations of methyl bromide in an agricultural valley and applications to exposure assessment, Atmospheric Environment 34 (2000) 3511–3523.
[13] H. Floesser-Mueller, W. Schwack, Photochemistry of organophosphorus insecticides, Reviews of Environmental Contamination and Toxicology 172 (2001) 129–228.
[14] S. Bondarenko, J.Y. Gan, Degradation and sorption of selected organophosphate and carbamate insecticides in urban stream sediments, Environmental Toxicology and Chemistry 23 (2004) 1809–1814.
[15] M. Franko, P. Trebse, L. Pogacnik, Laser-induced degradation of organophosphates and monitoring of their toxicity by cholinesterase biosensors, Critical Reviews in Analytical Chemistry 33 (2003) 285–290.
[16] E. Moctezuma, L. Elisa, P. Gabriela, H. de Las, Photocatalytic degradation of methyl parathion: reaction pathways and intermediate reaction products, Journal of Photochemistry and Photobiology A: Chemistry 186 (2007) 71–84.
[17] H.B. Wan, M.K. Wong, C.Y. Mok, Comparative-study on the quantum yields of direct photolysis of organophosphorus pesticides in aqueous-solution, Journal of Agricultural and Food Chemistry 42 (1994) 2625–2630.
[18] T. Kromer, H. Ophoff, A. Stork, F. Fuhr, Photodegradation and volatility of pesticides—chamber experiments, Environmental Science and Pollution Research 11 (2004) 107–120.
[19] N. Mikami, K. Imanishi, H. Yamade, J. Miyamoto, Photodegradation of fenitrothion in water and on soil surface, and its hydrolysis in water, Nippon Noyaku Gakkaishi 10 (1985) 263–272.
[20] J. Miyamoto, Degradation of Fenitrothion in Terrestrial and Aquatic Environments Including Photolytic and Microbial Reactions, 1977, pp. 105–134.
[21] T.M. Sakellarides, M.G. Siskos, T.A. Albanis, Photodegradation of selected organophosphorus insecticides under sunlight in different natural waters and soils, International Journal of Environmental Analytical Chemistry 83 (2003) 33–50.
[22] Q.Z. Zhang, X.H. Qu, W.X. Wang, Mechanism of OH-initiated atmospheric photooxidation of dichlorvos: a quantum mechanical study, Environmental Science & Technology 41 (2007) 6109–6116.
[23] L.S. Aston, J.N. Seiber, Fate of summertime airborne organophosphate pesticide residues in the Sierra Nevada mountains, Journal of Environmental Quality 26 (1997) 1483–1492.
[24] J.E. Woodrow, D.G. Crosby, T. Mast, K.W. Moilanen, J.N. Seiber, Rates of transformation of trifluralin and parathion vapors in air, Journal of Agricultural and Food Chemistry 26 (1978) 1312–1316.
[25] J.E. Woodrow, D.G. Crosby, J.N. Seiber, Vapor-phase photochemistry of pesticides, Residue Reviews 85 (1983) 111–125.
[26] A.M. Winer, R. Atkinson, Atmospheric reaction pathways and lifetimes for organophosphorous compounds, in: K. Da (Ed.), Long Range Transport of Pesticides, Chelsea, 1990, pp. 115–127.
[27] B.J. Finlayson-Pitts, J.N. Pitts, Chemistry of the Lower and Upper Atmosphere, 2000.
[28] N.-O.A. Kwamena, M.G. Staikova, D.J. Donaldson, I.J. George, J.P.D. Abbatt, Role of the aerosol substrate in the heterogeneous ozonation reactions of surface-bound PAHs, Journal of Physical Chemistry A 111 (2007) 11050–11058.
[29] A. Chukwudebe, R.B. March, M. Othman, A.T.R. Fukuto, Formation of trialkyl phosphorothioate esters from organophosphorus insecticides after exposure to either ultraviolet light or sunlight, Journal of Agricultural Food Chemistry 37 (1989) 539–545.
[30] R.L. Joiner, K.P. Baetcke, Identification of the photoalteration products formed from parathion by ultra violet light, Journal of the Association of the Official Analytical Chemistry 57 (1974) 408–415.
[31] J. Weber, R. Kurková, J. Klánová, P. Klán, C.J. Halsall, Photolytic degradation of methyl-parathion and fenitrothion in ice and water: implications for cold environments, Environmental Pollution (2009), doi:10.1016/j.envpol.2009.05.045.
[32] T.W. Chou, R. Spanggord, E. Shingai, N. Bohonos, Fate of methyl parathion in freshwater systems. 3. Biodegradation studies, Abstracts of Papers of the American Chemical Society 172 (1976) 62–162.
[33] N.O. Crossland, D. Bennett, Fate and biological effects of methyl parathion in outdoor ponds and laboratory aquaria. 1. Fate, Ecotoxicology and Environmental Safety 8 (1984) 471–481.
[34] S.V. Dzyadevych, J.M. Chovelon, A comparative photodegradation studies of methyl parathion by using Lumistox test and conductometric biosensor technique, Materials Science & Engineering C: Biomimetic and Supramolecular Systems 21 (2002) 55–60.
[35] Z. Gerstl, C.S. Helling, Fate of bound methyl parathion residues in soils as affected by agronomic practices, Soil Biology & Biochemistry 17 (1985) 667–673.
[36] S.S. Lee, B.R. Holt, B.E. Suta, D.H. Liu, Fate of methyl parathion in freshwater systems. 4. Environmental fate assessment, Abstracts of Papers of the American Chemical Society 172 (1976) 63–163.
[37] W.R. Mabey, A. Baraze, B.Y. Lan, H. Richardson, D.G. Hendry, T. Mill, Fate of methyl parathion in freshwater systems. 2. Hydrolysis and photolysis, Abstracts of Papers of the American Chemical Society 172 (1976) 61–161.
[38] H.K. Rotich, Z.Y. Zhang, Y.S. Zhao, J.C. Li, The adsorption behavior of three organophosphorus pesticides in peat and soil samples and their degradation in aqueous solutions at different temperatures and pH values, International Journal of Environmental Analytical Chemistry 84 (2004) 289–301.
[39] J.H. Smith, D.C. Bomberger, D.L. Haynes, D.F. Stivers, M.E. Zinnecker, Fate of methyl parathion in freshwater systems. 1. Introduction and physical transport processes, Abstracts of Papers of the American Chemical Society 172 (1976) 60–160.

[40] M. Segal-Rosenheimer, Y. Dubowski, Photolysis of thin films of cypermethrin using in situ FTIR monitoring: products, rates and quantum yields, Journal of Photochemistry and Photobiology A: Chemistry 200 (2008) 262–269.
[41] D Lin-Vien, N.B. Colthup, W.G. Fateley, J.G. Grasselli, The Handbook of Infrared and Raman Frequencies of Organic Molecules, Academic Press, 1991.
[42] M. Janotta, K. Manfred, F. Vogt, B. Mizaikoff, Sol–gel based mid-infrared evanescent wave sensors for detection of organophosphate pesticides in aqueous solution, Analytica Chimica Acta 496 (2003) 339–348.
[43] S. Buckland, R. Davidson, The photodegradation of parathion and chlormephos, Pesticide Science 19 (1987) 61–66.
[44] M. Segal-Rosenheimer, Y. Dubowski, Heterogeneous ozonolysis of cypermethrin using real-time monitoring FTIR techniques, Journal of Physical Chemistry C 111 (2007) 11682–11691.
[45] N. Daneshvara, M.A. Behnajadyb, Y.Z. Asgharb, Photooxidative degradation of 4-nitrophenol (4-NP) in UV/H_2O_2 process: influence of operational parameters and reaction mechanism, Journal of Hazardous Materials 139 (2007) 275–279.